POTSDAM-INSTITUT FÜR KLIMAFOLGENFORSCHUNG

Water Resources Research

RESEARCH ARTICLE
10.1029/2018WR024111

Assessing Hydrograph Similarity and Rare Runoff Dynamics by Cross Recurrence Plots

Dadiyorto Wendi[1,2,3], **Bruno Merz**[1,2], **and Norbert Marwan**[3]

[1]Institute of Earth and Environmental Science, University of Potsdam, Potsdam, Germany, [2]Section 5.4 Hydrology, German Research Centre for Geosciences (GFZ), Potsdam, Germany, [3]Potsdam Institute for Climate Impact Research (PIK), Potsdam, Germany

Key Points:
- This manuscript presents the first application of recurrence plots in catchment hydrology
- CRP is used as a novel method for quantifying comprehensive hydrograph similarity based on runoff dynamics
- Time delay embedded phase space trajectory allows to consider relationships between magnitudes of different point in time

Correspondence to:
D. Wendi,
dadiyorto@outlook.com

Citation:
Wendi, D., Merz, B., & Marwan, N. (2019). Assessing hydrograph similarity and rare runoff dynamics by cross recurrence plots. *Water Resources Research*, *55*, 4704–4726. https://doi.org/10.1029/2018WR024111

Received 18 SEP 2018
Accepted 12 MAY 2019
Accepted article online 17 MAY 2019
Published online 7 JUN 2019

Abstract This paper introduces a novel measure to assess similarity between event hydrographs. It is based on cross recurrence plots (CRP) and recurrence quantification analysis (RQA), which have recently gained attention in a range of disciplines when dealing with complex systems. The method attempts to quantify the event runoff dynamics and is based on the time delay embedded phase space representation of discharge hydrographs. A phase space trajectory is reconstructed from the event hydrograph, and pairs of hydrographs are compared to each other based on the distance of their phase space trajectories. Time delay embedding allows considering the multidimensional relationships between different points in time within the event. Hence, the temporal succession of discharge values is taken into account, such as the impact of the initial conditions on the runoff event. We provide an introduction to cross recurrence plots and discuss their parameterization. An application example based on flood time series demonstrates how the method can be used to measure the similarity or dissimilarity of events, and how it can be used to detect events with rare runoff dynamics. It is argued that this methods provides a more comprehensive approach to quantify hydrograph similarity compared to conventional hydrological signatures.

1. Introduction

The shape of flood event hydrographs can vary substantially between regions and between events for a given catchment, depending on catchment and event characteristics. Variations in hydrographs can be expected for different event types, for example, driven by different climatic factors, and for different catchment conditions. For instance, short-rain floods triggered by moderate to substantial rainfall tend to show a faster response compared to snowmelt driven floods (Merz & Blöschl, 2003). Hence, the hydrograph is a fingerprint of the processes involved in the rainfall-runoff event (Blöschl et al., 2011). Quantifying the similarity or dissimilarity of event hydrographs has received increasing attention in the field of surface water hydrology (Haaf & Barthel, 2018), for example, within the "Predictions in Ungauged Catchments" initiative (Hrachowitz et al., 2013), or for assessing the performance of hydrological models (Ehret & Zehe, 2011).

A range of indices, herein also called hydrological signatures, have been used to describe rainfall-runoff event hydrographs. The hydrograph peak (Q_p) is the most popular hydrological signature in flood risk assessment and flood design due to its close relationship with the socioeconomic impact of floods. Other important hydrological signatures are discharge volume (V), event duration (t_d), time to peak (t_p), recession time (t_f), base flow index (BFI), or the rising and falling limb slope of the hydrograph (ΔQ_{rise} and ΔQ_{fall}). These signatures have been used as event similarity indices required for classification, regionalization, prediction, change and extreme event analysis, and model calibration (Bárdossy, 2006; Merz & Blöschl, 2003; Peel & Blöschl, 2011; Sawicz et al., 2014; Westerberg & McMillan, 2015; Westerberg et al., 2016). However, these indices either represent a single element of the hydrograph only (Q_p, t_d, t_p, and t_f) or they are a statistical aggregate of the hydrograph (V, BFI and ΔQ_{rise}, and ΔQ_{fall}). Other studies have introduced the consideration of multivariate signatures altogether to better exploit the information contained in the hydrograph, for example, the studies of Brunner et al. (2017), Hannah et al. (2000), Ehret and Zehe (2011), and Ternynck et al. (2016).

In this study we propose a more elaborate hydrological signature to quantify similarity between event hydrographs. Our signature is based on the phase space representation of discharge hydrographs and attempts

to consider the event runoff dynamics more comprehensively. Instead of using a single element index or a joint considerations of statistical aggregates of the hydrograph signatures, it considers the entire, continuous hydrograph shape, that is, the time sequence and additionally its dependence on the antecedent conditions of the flood event.

In our approach a phase space trajectory is reconstructed from the corresponding hydrograph using Taken's time delay embedding method (Takens, 1981). Please note that the official term "reconstruct" is used instead of "construct" because the theory claims that this embedding allows recreating the system behavior, represented by the phase space geometry, by just using the time series of one of the system variables (Packard et al., 1980; Takens, 1981). However, we apply the embedding method in a more practical manner, such that the reconstructed phase space trajectory allows the analysis of the multidimensional relationship between discharge values in different points in time. This means that we can implicitly consider antecedent conditions of the flood, that is, discharge values prior to the flood peak. Their consideration are important for flood analysis, as for instance, a moderate rainfall prior to a flood may partially saturate the catchment and lead to a high flood event peak—much higher than would be expected from the event precipitation alone.

The specific method we propose are cross recurrence plots (CRPs), as a variation of recurrence plots (RPs), and their quantification (recurrence quantification analysis [RQA]) as the basis for quantifying hydrograph similarity. RP and RQA are used in order to visualize and quantify phase space trajectories especially at higher dimensions where such trajectories cannot be visualized anymore (Marwan et al., 2007). Both RP and RQA have gained considerable popularity over the past decades in several scientific disciplines, from economy, physiology, neuroscience, paleoclimatology, astrophysics to engineering, especially when focusing on nonlinear time series analysis and characterizing the behavior of complex systems (Aceves-Fernandez. et al., 2012; Carrubba et al., 2010; Crowley, 2008; Eroglu et al., 2016; Goswami et al., 2018; Marwan & Meinke, 2004; Oberst & Lai, 2015). However, to the authors' knowledge, RP, CRP, and RQA have not been used in catchment hydrology, let alone in comparing hydrograph dynamics, despite the popular exploration of chaos theory, which also builds on phase space trajectories. Such phase space trajectories, for example, have been used for hydrological forecasting or gap filling of hydrological time series (Sivakumar, 2000).

This paper introduces CRP as a novel approach for assessing the similarity or dissimilarity of rainfall-runoff events based on the phase space representation of their hydrographs. We argue that this approach better captures the underlying runoff dynamics compared to the traditional hydrological signatures. Not only the comparison method is based on the entire shape of hydrograph but also configurable to capture the relationships of magnitudes at different time through time delay embedding. Since such methodological application in catchment hydrology has no references yet, the paper first provides a practical introduction to CRP and RQA. To introduce the methodology, we contrast it with the traditional way of comparing time series, that is, through correlation analysis using scatter plots and correlation coefficients. It is important to note that, in contrast to correlation analysis, CRP and RQA are not restricted to comparing time series of the same length.

Our application example, using historical floods at the Elbe River runoff station at Dresden, Germany, compares flood events of varying durations that occurred in February and March during the period 1901–2010. These two months show the highest number of annual maxima at the gauge Dresden. The application example illustrates the potential of the method to quantify similarity of hydrographs between events and to detect their unusual runoff dynamics. This could be events with unseasonal runoff dynamics, that is, an unexpected flood type for a certain season, or events with rare event characteristics, that is, never seen before runoff dynamics.

We see the potential of this method to be used for a wide range of questions in hydrology. An obvious extension would be to quantify the similarity of longer epochs, for example, annual periods, instead of flood events. Another example would be the detection and attribution of change in hydrological time series by investigating whether changes in the runoff dynamics can be identified.

2. Methodology

2.1. Cross Recurrence Plot (CRP)

The CRP is a variation of the RP. RP was first introduced by Eckmann et al. (1987) to visualize the recurrence behavior and properties of dynamical systems through their phase space topology. A dynamical system is represented by a phase space trajectory, and RP is used to identify recurring states of this system, that is, whether a certain pattern recurs in time. This recurring states are represented by the diagonal lines in the

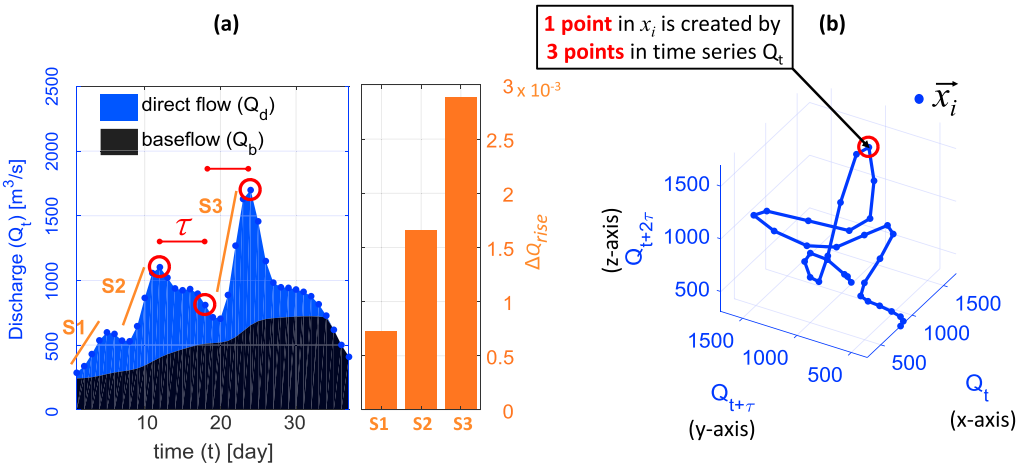

Figure 1. Multiple-peak flood event (a) and its three-dimensional phase space reconstruction (b). The phase space vector consists of three dimensions, whereas each axis shows the values of the original hydrograph separated by the time delay τ and 2τ. Red circles show exemplarily the reconstruction for one point in the phase space.

two-dimensional plot where x and y axes represent time. In contrast, CRP is a tool to analyze time synchronization and similarity between two time series by comparing their phase space trajectories that can also be reconstructed through time delay embedding (Marwan, Thiel, et al., 2002).

In CRP, continuously connected points that form diagonal lines indicate that (parts of) the time sequence patterns of the two hydrographs are similar to each other. Hence, the longer these diagonal lines, the longer are the patterns that are similar between the hydrographs. Time delay embedding can also be additionally implemented to allow the reconstruction of a high-dimensional phase space trajectory from univariate time series. This means that multiple subsets of values within a single time series are extracted according to a time delay τ and plotted in the phase space to describe the relationships of magnitudes at different time distanced by τ.

For instance, a two-dimensional phase space vector can be compared to an autocorrelation scatter plot where the x and y axes are the subset values of the original time series that are separated by a shift of τ. A three-dimensional phase space contains a third variable, that is, x, y, and z with time delay of τ and 2τ, and so on for higher dimensions. Figure 1a shows an extracted flood hydrograph with three peaks or subevents. The rising slope at each subevent i (defined as the gradient from the start of the subevent to its peak) is higher for the second and third peaks. This can be explained mainly by the increasing wetness of the catchment from the first to the third subevent. This kind of cascading relationships in time where the initial or antecedent conditions are important information motivates the use of multidimensional, time delay embedded, phase space analysis.

This time delay phase space reconstruction follows Takens' embedding theorem (Packard et al., 1980; Takens, 1981):

$$\vec{x}_i = (u_i, u_{i+\tau}, \ldots, u_{i+(m-1)\tau}), \tag{1}$$

where m is the embedding dimension and τ is the time delay, and u_i is a univariate time series or in this case our discharge series (Q_t).

When comparing two time series, phase space trajectories (x_i and y_j) are reconstructed from both time series, and the pointwise similarity of the two trajectories can be assessed based on their distance and visualized with CRP (see Figure 2). The CRP is a two-dimensional matrix encoding the similarity structure of two high-dimensional, embedded systems. It is a visual representation of a rectangular matrix in which the matrix elements (recurrence points $CR_{i,j}(\varepsilon)$) correspond to times at which the states (i,j) of the two dynamical systems are equal or similar (defined by their phase space distance and a threshold ε):

$$CR_{i,j}(\varepsilon) = \begin{cases} 1, \text{ if } \|\vec{x}_i - \vec{y}_j\|_2 < \varepsilon \\ 0, \text{ otherwise} \end{cases} \qquad i = 1, \ldots, N, \quad j = 1, \ldots, M, \tag{2}$$

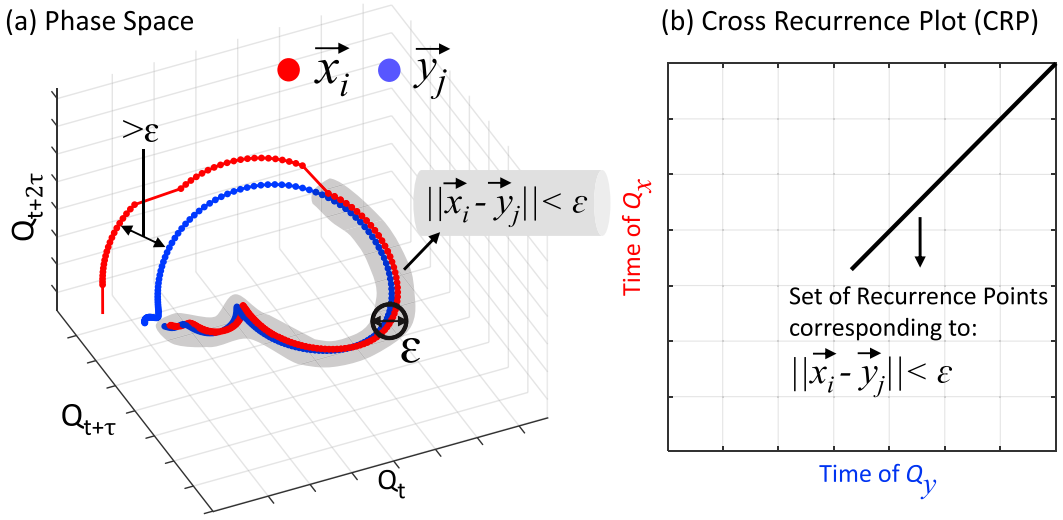

Figure 2. Comparison of two phase space trajectories $\vec{x}_i$ and $\vec{y}_j$ constructed from time series Q_x and Q_y using distance threshold ε (a) to define recurrence points in the CRP (b).

where N and M are the number of measured points in the compared phase space vectors $\vec{x}_i$ and $\vec{y}_j$, ε is a cutoff threshold for distances between the vectors, and $\|\cdot\|_2$ is the Euclidean norm.

To exemplify the concept of CRP and to demonstrate its differences to the widely used tools scatter plot and cross-correlation analysis, Figure 3 compares two hydrographs using scatter plots and CRP. One of the differences between the CRP and the scatter plot is that the scatter plot axes represent magnitudes, while in the CRP they represent the time of occurrence of the two series. When two identical time series are compared, CRP shows a single diagonal line (45° angle) that divides the CRP matrix symmetrically (Figure 3.1c, green line). As differences increase, this straight diagonal line will become more and more distorted, for example, becoming perforated and wiggled. Then this line could be quantified by *DET* in order to derive a similarity measure (section 2.2). Further, it is worth to note that the high-dimensional embedding results in embedding loss with a size of $(m-1)\tau$. This embedding loss is a result of reconstructing the phase space vectors corresponding to the number of dimension (m) and time delays (τ), and thus, the size of the CRP is shorter by $(m-1)\tau$ and needs to be cautioned.

The first example shows the CRP when comparing two identical hydrographs patterns Q_a and Q_b, which occur at different times; that is, Q_b is shifted by 17 time units (Figure 3.1a). Despite the time shift, the CRP still indicates the similarity of the two time series as indicated by the diagonal line. In addition, this diagonal line also indicate the amount of the time shift. This similarity cannot be derived from the scatter plot without knowing the time shift in advance. Hence, the scatter plot and correlation analysis (Pearson correlation coefficient $R = 0.17$) could lead to the wrong conclusion that there is no similarity between Q_a and Q_b. The CRP approach is useful for detecting recurring runoff dynamics, possibly related to the same causative mechanism, which do not necessarily happen at the same season. It should also be noted that the CRP is useful for comparing hydrographs regardless of their, possibly dissimilar, duration.

The second example compares Q_a with a random system dynamics where Q_b is a randomly shuffled time sequence of Q_a (Figures 3.2a–3.2c). In this case, the CRP does not show any diagonal lines. Similarly, the scatter plot does not indicate a relationship, but it should be cautioned that the correlation analysis suggests a substantial anticorrelation (Pearson correlation coefficient $R = -0.28$).

The third example (Figures 3.3a–3.3c) compares two hydrographs with different runoff dynamics where Q_b represents an increased storage capacity in the catchment that dampens the flow. This could result from a perturbation to the catchment such as dam construction. Q_b is obtained by a storage-based Muskingum transformation that is commonly used for flow routing in hydrological modeling (Hattermann et al., 2014). The parameters of the Muskingum transformation are set as follows: storage constant $K = 15$ time units; weighting factor $x = 0.01$. Due to the different runoff dynamics, the resulting CRP shows a rather high

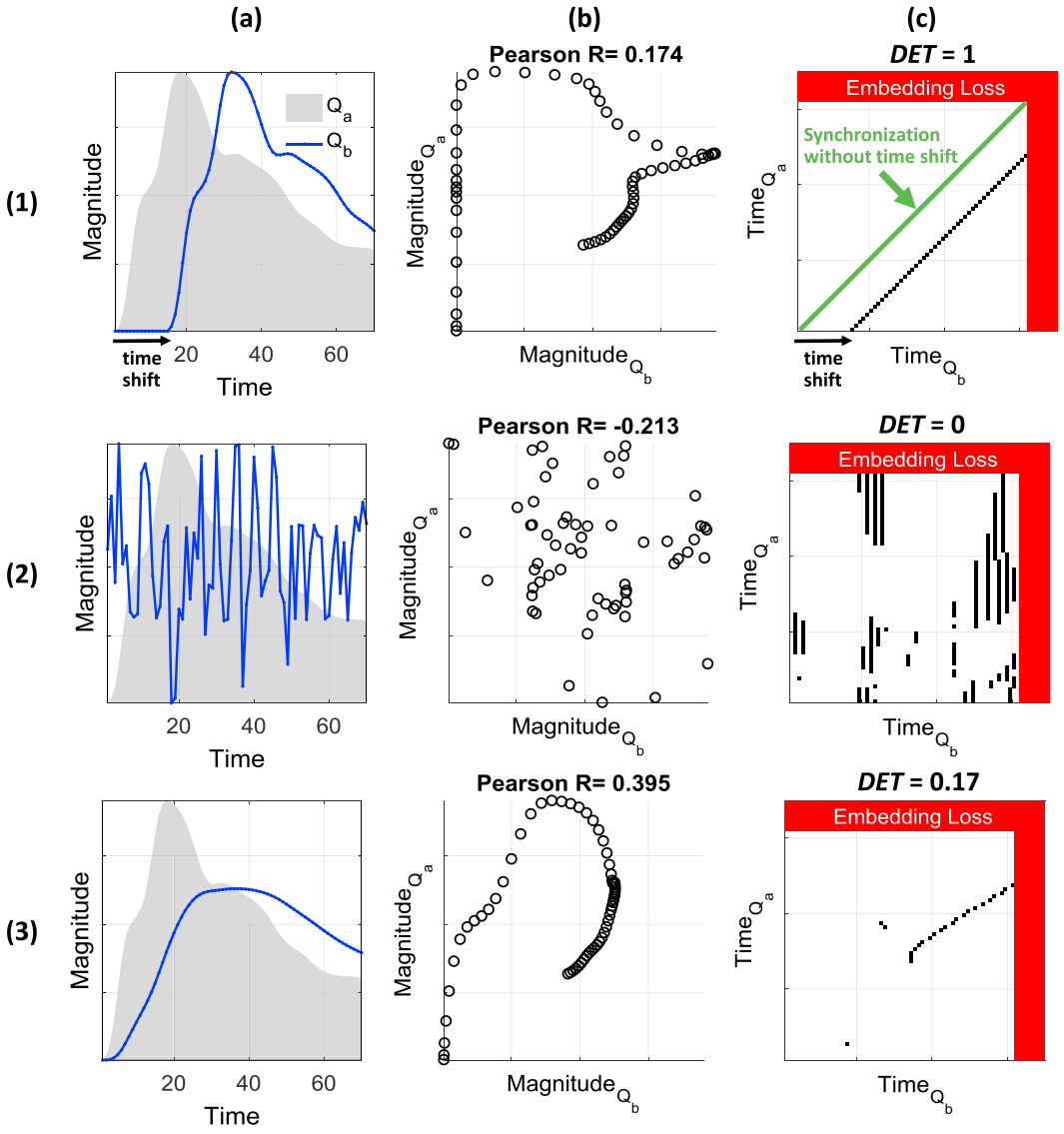

Figure 3. Comparison of two discharge time series (a) with scatter plot and correlation coefficient R (b) and cross recurrence plot and *determinismDET* (c). Example 1 compares two identical hydrographs with a shift in their timing, example 2 compares a hydrograph with a randomly shuffled version of the same hydrograph, and example 3 compares two different runoff dynamics where Q_b results from a storage-based Muskingum transformation of Q_a representing an increased storage capacity in the catchment. The embedding losses are shaded in red.

dissimilarity in contrast to the substantial correlation coefficient $r \approx 0.4$. Although this CRP contains an inclined line, this line is rather broken and not tilted with 45°, which would indicate similarity.

Furthermore, It is important to note that, unlike correlation analysis and scatter plots, CRP and RQA do not require that the two time series have the same length. In the case of cross-correlation analysis the lag would be constant for the complete piece of time series, where CRP allows temporal changes of the temporal relationship between the two considered time series and, thus, also nonmonotonic changes in the relationship.

When working with real world observations, the presence of noise might cause the diagonal in CRP to be discontinuous. Two examples are given Figure 4, where the hydrograph Q_a is compared to similar hydrographs that have been constructed by imposing white Gaussian noise on Q_a with a signal-to-noise ratio of 25 and 20 dB, respectively. These values are represented in decibels (dB), a logarithmic ratio between the signal and noise level. The diagonal line of the CRP becomes broken or contains gaps, and these gaps are larger

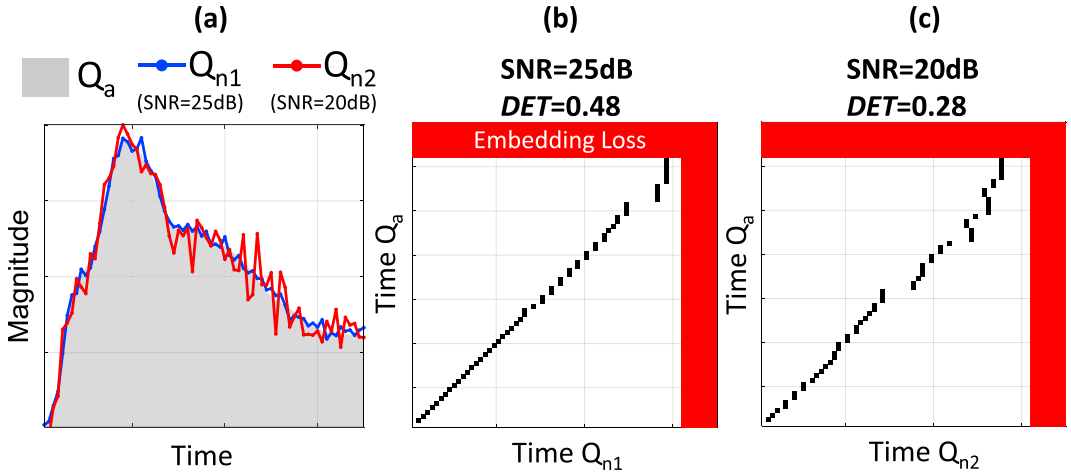

Figure 4. Comparison of a hydrograph with noise-induced versions of the same hydrograph (a). Cross recurrence plot for a signal-to-noise ratio (SNR) of 25 dB (b) and 20 dB (c), respectively.

when the signal is more noisy. When dealing with noisy signals, one can consider noise reduction methods, such as filtering or smoothing; for an overview see Elshorbagy et al. (2002).

2.2. Recurrence Quantification Analysis

Similar to the correlation coefficient that summarizes the information of a scatter plot, patterns within a CRP can be quantified by RQA. In our study, RQA is used to provide a similarity index for flood hydrographs. RQA can also be used to reveal typical dynamical features of the investigated system, such as range of predictability, chaos-order, and chaos-chaos transition (Marwan, Wessel, et al., 2002; Trulla et al., 1996). The RQA measure *determinism* (*DET*) describes the similarity (or dissimilarity) of two dynamical systems using the distribution of connected recurrence points that form diagonal lines, that is, lines in the CRP with slope 45°, over all the points within the CRP:

$$DET = \frac{\sum_{l=l_{\min}}^{N} lP(l)}{\sum_{i,j}^{N} CR_{i,j}}, \tag{3}$$

where $P(l) = \{l_i; i = 1, \ldots, N_l\}$ is the relative frequency of the lengths l of diagonal structures, N_l is the total number of those diagonal lines in the CRP, and $l_{\min}$ is the minimum length of diagonal lines (usually two recurrence points).

This quantification based on the fraction of diagonal lines among all recurrence points ($CR_{i,j}$) considers the influence of scattered single recurrence points that occur by chance. *DET* varies between 0 and 1, indicating the range from low to high similarity in the dynamics of the two times series. For similar continuous dynamical systems, many diagonal lines in the CRP are typical, leading to a high value of *DET* (Marwan, 2010). The similarity of the two continuous states in the phase space is strictly defined by the 45° diagonal line, and any other lines are not relevant for the quantification of similarity. Single, isolated recurrence points can occur if states are rare, if they do not persist, or if their distance fluctuate heavily. For instance, two signals with the same magnitudes but different time sequence, and hence different dynamics, would lead to single points and result in a low *DET*. For the two identical but shifted hydrographs (Figure 3.1), *DET* is 1. Hence, this measure correctly identifies the identical runoff dynamics of the two hydrographs in contrast to the correlation coefficient that suggests little similarity ($R = 0.17$). This is because correlation analysis is unable to capture the nonmonotonic pattern in the scatter plot. When comparing the hydrograph with its randomly shuffled version (Figure 3.2), $DET = 0$ in contrast to the, possibly misleading, value of the correlation analysis ($R = -0.28$).

When comparing the two hydrographs with different runoff dynamics in Figure 3.3, *DET* shows a low value of 0.17 suggesting little similarity in contrast to the correlation analysis ($R \approx 0.4$).

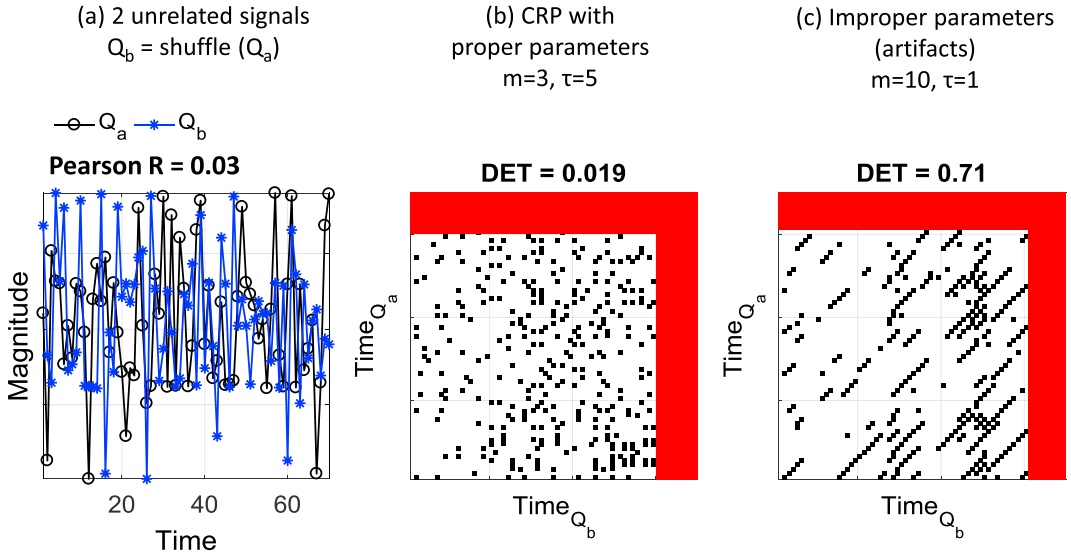

Figure 5. Example of artifacts in cross recurrence plot (CRP) due to improper embedding parameters: comparing (a) two unrelated random signals result in (b) CRP with proper embedding parameters and (c) CRP with artifacts caused by improper parameters.

2.3. Construction and Parameterization of CRP

Three parameters are required in constructing the CRP. These are the two parameters for the time delay embedding, that is, embedding dimension m and time delay τ, as well as the phase space distance threshold ε that defines a recurrence point. In a specific context, m and τ can be chosen according to the requirement of the analysis, that is, by the number of interrelated points in time. For example, the description of events consisting of complex, multipeak hydrographs would require a higher number of points than regular events. The subevents within a multipeak hydrograph have possibly different characteristics. Initial subevents, for instance, can be regarded as antecedent conditions and might affect the following subevents, that is, increase their magnitude. Therefore, their relationships are valuable in the characterization of the event dynamics. In general, the higher the embedding dimension and the smaller the time delay, the more complete the dynamics can be described by the phase space trajectories. However, artifacts from the suboptimal choice of parameters and embedding loss, which also increases with higher m and τ, should be avoided. Two unrelated random signals for instance (Figure 5a) should yield zero or near zero value of *DET* and be represented by scattering recurrence points in the CRP (Figure 5b), but improper parameters could artificially increase number of diagonal lines and hence result in artifacts, that is, high *DET* value (Figure 5c).

The standard approaches for finding the optimal embedding parameters are the method of false nearest neighbors for m and the autocorrelation or mutual information for τ (Fraser & Swinney, 1986; Kantz & Schreiber, 2005; Kennel et al., 1992). However, Marwan (2010) concludes that τ is sometimes overestimated by autocorrelation and mutual information and that the choice of m has to be considered with care, as a wrong choice artificially increases diagonal lines and *DET* values.

To prevent such artifacts, we have proposed a random shuffling method to determine the safe region of embedding parameters (Wendi et al., 2018). However, this method was developed for the RP assessing the recurring dynamics within a single system or time series. Here, we adapt this method for the CRP by comparing two identical time series and shuffling the time sequence of only one of the two time series. The basic idea is, similar to the CRP example of Figure 3.2, that shuffling destroys the original sequence information about the process, thus changing its dynamics to a different and random one. The *DET* value from the CRP of the hydrograph Q_a and the shuffled one Q_b should be small. A high *DET* value for a certain set of parameters m and τ indicates that the CRP contains artificially long diagonal lines and, therefore, this parameter set is assumed to be unsafe. Safe parameter sets can be found using a *DET* distance matrix. The *DET* distance is the absolute difference between the *DET* values of the original CRP, that is, constructed from the two identical time series without shuffling, where *DET* is expected to be 1, and multiple iterations of shuffling, with expected low *DET* values. These multiple iterations are then summarized based on the median. The median

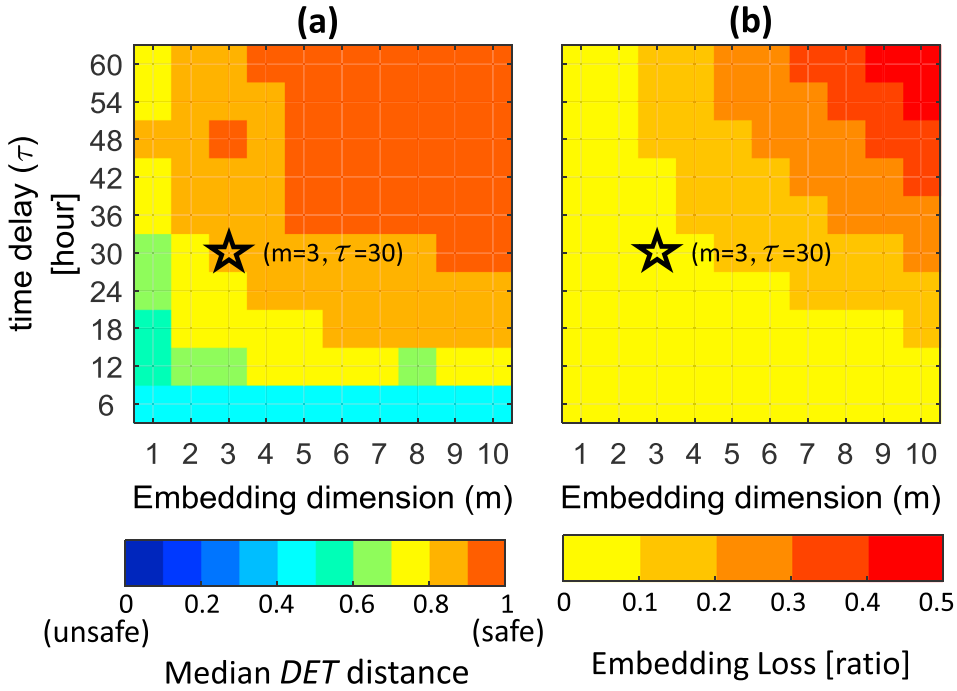

Figure 6. Safe regions and optimal parameter sets: (a) median *DET* distance and (b) embedding loss. The parameter set used in this study is marked with a star.

DET distance varies from 0 to 1; the larger the *DET* distance, the safer the parameter set. The optimal choice is a trade-off between the requirements for a safe parameter region and for small embedding loss.

To demonstrate the parameterization of CRP, we use the hydrograph example in Figure 1. It has a daily resolution but is resampled with linear interpolation to a finer resolution of 6 hr to allow the evaluation of higher embedding parameters (m and τ). We calculate the median of the *DET* distances for 100 shuffling iterations for each set of embedding parameters within the range of $1 \leq m \leq 10$ and $6 \leq m \leq 60$ hr (Figure 6a) and the resulting embedding loss, that is, ratio of the loss to the time series length (Figure 6b). We select the parameter set from the region with high median *DET* distances (above 0.8) and small embedding loss (below 10%). In this example, since we have decided to fix the embedding dimension m to 3, therefore, best candidates for τ selection derived from this safe parameter region are 30 and 40 hr. Should a higher m be desired in order to quantify the relationship of more points in time, then τ should be adjusted to match the mentioned trade-off.

In addition to the embedding parameters, an optimal threshold for the phase space distance ε is also essential to prevent artifacts. Thick lines, for instance, can easily occur in continuous dynamical systems due to the temporal correlation of the phase space trajectory, causing the CRP to contain redundant information when ε is not defined properly (Krämer et al., 2018; Schultz et al., 2011; Wendi & Marwan, 2018). Figure 7 illustrates this problem for the hydrograph comparison in Figure 3.1. Subfigure (a) shows the distance matrix of the two phase space vectors ($\|\vec{x}_i - \vec{y}_j\|$), while subfigure (b) shows exemplary three slices of the distance matrix at rows 20, 40 and 60, that is, distances relative to Q_a at time 20, 40, and 60. Using simply a distance threshold ε in defining the recurrence points leads to thick lines in the CRP for those periods where the local variance of the hydrograph is low, that is, at the time of Q_b around 40-50 (Figure 7c). Such thick lines artificially increase the number of diagonal lines, yielding unreasonably high *DET* values. Schultz et al. (2011) and Wendi and Marwan (2018) suggested a local minima-based recurrence definition to solve this problem. The minima are found in each row of the distance matrix and should correspond to the closest neighbors of a state within the threshold ε. This method minimizes the line thickness (compare Figures 7c and 7d) and requires much less computational effort compared to alternative solutions (Schultz et al., 2011). Moreover, Schultz et al. (2011) shows that the local minima-based CRP is less dependent on the selection of the threshold ε, making the method more robust. Therefore, we select and recommend this method for calculating the CRP for comparing runoff dynamics.

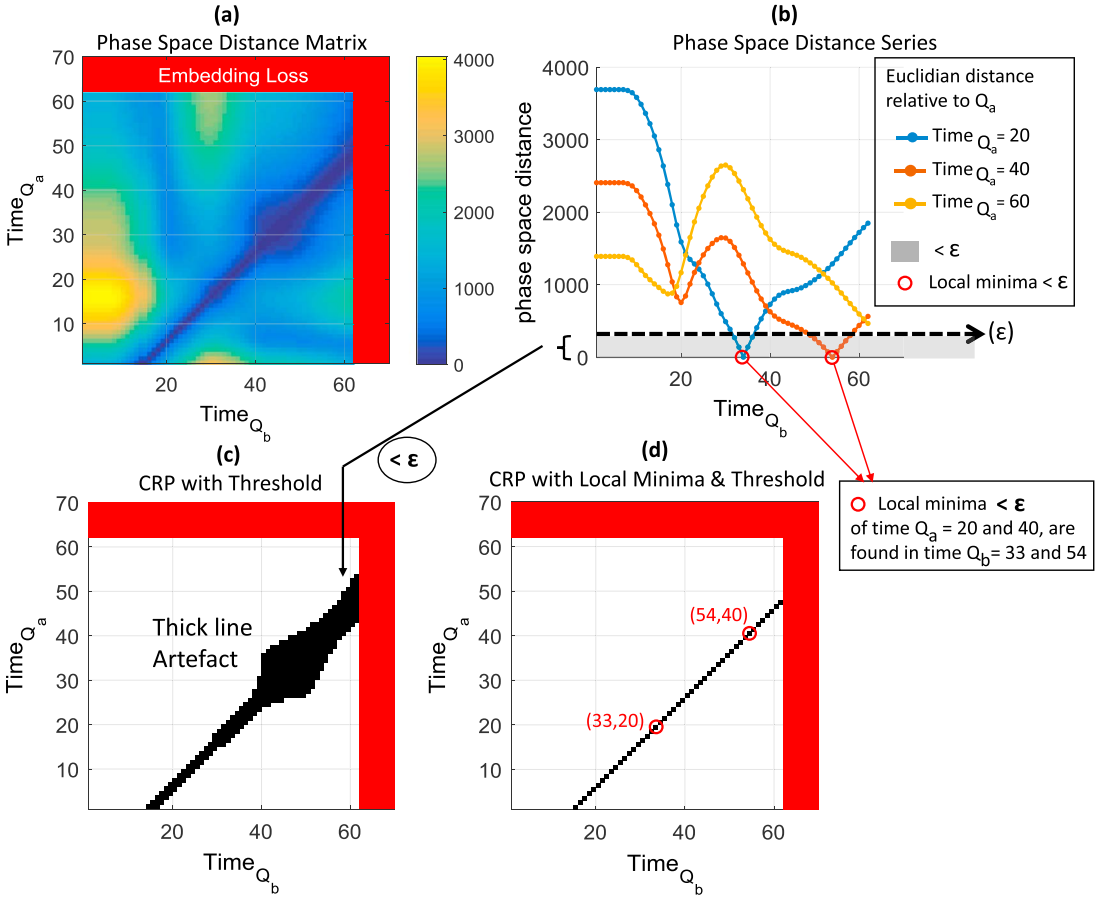

Figure 7. Illustration of the local minima approach (Schultz et al., 2011; Wendi & Marwan, 2018) to define recurrence points for the cross recurrence plot (CRP) example shown in Figure 3.1. (a) Recurrence distance matrix ($\|\vec{x}_i - \vec{y}_j\|$); (b) phase space distance with reference to Q_a at time 20, 40, and 60; and their corresponding local minima below the applied threshold (ε = 5th percentile). (c and d) CRPs resulting from the distance matrix below the threshold and from the local minima below the threshold, respectively.

3. Application Example and Comparison with Conventional Indices

We apply CRP and RQA to evaluate the similarity of flood hydrographs measured at Dresden gauge from 1901 to 2010. This gauge is located in the city of Dresden, Germany, on the Elbe River, which flows from the Krkonoše Mountains in the Czech Republic to the North Sea at Cuxhaven, Germany. This application is meant to show the potential of the method to quantify similarity taking into account the underlying runoff dynamics and to detect unusual events. We also compare the results with frequently used hydrological signatures individually and and altogether. Using this example, we attempt to provide a practical introduction to CRP and RQA, as these methods have not been used in hydrology so far but have been beneficial in several other disciplines.

To compile a set of flood events, we first identify the annual maximum values from the times series of daily streamflow observations. Thereafter, we select only those events with peaks in February and March. These are the months where the highest number of annual streamflow maxima occur. Although the same flood types, for example, snowmelt flood or rain-on-snow flood, may occur in these months, February and March are often classified in different seasons, that is, December–February for winter and March–May for spring (Matti et al., 2017). Hence, it is interesting to our analysis to which extent events with similar dynamics occur in these two months. We further select only those events with a peak of at least 1,000 m^3/s to exclude minor events. The next step consists in deriving the complete event hydrograph for each selected peak. To this end, we partition the streamflow into direct flow and base flow using the Boughton two-parameter separation method (Boughton, 1993). The start of the flood event is defined as the day when the direct flow reaches a minimum threshold of 50 m^3/s within 30 days prior to the peak flow. The event ends when the

direct flow falls below a second threshold of 30 m^3/s within 40 days after the peak. These thresholds have been subjectively determined after multiple trials with visual inspection. This procedure results in a series of 45 event hydrographs (shown in Figure C1 in Appendix C.

The first analysis of this event set compares the event in February 1953, which has a commonly seen single-peak hydrograph, with all other flood events in a pairwise manner. We construct the CRP for each hydrograph pair and use the *DET* measure as similarity index. For the CRP construction in this application example, we choose $m = 3$ to allow the visual comparison of the reconstructed phase space, and $\tau = 30$ hr. This parameter set is considered as a safe choice for all events. It is determined via the *DET* distance (section 2.3), that is, by comparing each event hydrograph to itself and its shuffled versions and by ensuring that the embedding loss does not exceed 10%. Each event's median *DET* distance is calculated for different parameters sets. In appendix A we provide the median *DET* distances for all 45 events based on the selected parameter set ($m = 3$; $\tau = 30$ hr), and the possible maximum *DET* distance for different parameter sets. For our fixed parameter set, all median *DET* distances fall into a considerable safe range, that is, above 0.6, and the majority is above 0.8. It would be possible to maximize our *DET* distances by changing their parameter sets, but this would require higher embedding dimension (m). For instance, for the events 1937 and 1942, a higher *DET* distance could be attained by increasing m to 5. Overall, longer multipeak events tend to have lower *DET* distance for the fixed parameter set and would require higher m values to maximize their *DET* distance. Although in this example m is fixed to 3 for the purpose of phase space visualization, it is recommended to utilize parameter sets that yield the maximum median DET distance for a more reliable assessment.

Figure 8 shows the time series of resulting *DET* values. Two events with high *DET* values, suggesting high similarity to the 1953 event, are exemplary shown in Figure 8c (February 1916) and Figure 8e (March 1969). Just like the 1953 event, their hydrographs consist of a single peak with similar shape. In contrast, the comparison with the event in February 1937 (Figure 8d) results in a low *DET* value as expected by the very different hydrograph shape with multiple peaks and considerably longer duration. A low *DET* value is also noticed for the March 1992 event (Figure 8f); this time the hydrograph slope is milder with lower flow magnitude. Figures 8g to 8k show the phase space trajectories for these four pairwise comparisons. They illustrate that the phase space trajectories of the events in 1916 and 1969 are much more similar to the 1953 event compared to the events in 1937 and 1992. Figure 8l–8o plot the CRPs for these four event pairs; the comparison with 1916 and 1969 shows extended 45° diagonal lines. In contrast, the CRP of 1937 shows several short lines, however only the first one has an angle of 45°. The CRP of 1969 consists of a single extended line; however, this line has a smaller than 45° angle. Note that the CRPs shown here are no longer square due to the different duration of the compared time series in the x axis, which is one of the advantages of using CRP approach.

This example of assessing the pairwise similarity of hydrographs can be extended to evaluate the rarity of each flood in terms of its runoff dynamics by intercomparing it to all other floods in the event set. This results in a matrix of *DET* values of all pairwise hydrograph intercomparisons (see Figure B1 in Appendix B), which can be summarized statistically. Figure 9 shows such an intercomparison; each flood hydrograph of February and March from 1901 to 2010 is compared to all the other events, and the median *DET* value is used as rarity measure. Events with low median *DET* values have hydrograph shapes that reoccur rarely within the event set, whereas high values suggest that these events have common hydrograph shapes. In case the hydrograph shape is a signature of the underlying flood generation processes, then the median *DET* value can be used to indicate unusual events in terms of flood generation. The two events with the highest and lowest median *DET* values, respectively, are marked in Figure 9a, and their hydrographs and phase space trajectories are shown in Figures 9b–9e and Figure 9h. In addition, the peak discharge and the median *DET* values of all events are plotted against their empirical exceedance probability in Figures 9f and 9g.

The 1940 event (Figure 9c) has the lowest median *DET* value (zero), indicating that this is the most unusual event in the whole flood series. It contains a first peak whereas the increase and recession are very steep and the peak magnitude shows the highest value of all February and March events of the period 1901–2010. Its second peak has completely different characteristics. After a steep increasing limb the hydrograph shows almost constant values for 10 days. The historical archive (Schuh, 2011) reports that this event was a rare ice jam flood caused by accumulated ice debris slightly downstream of the gauging station. The unusual

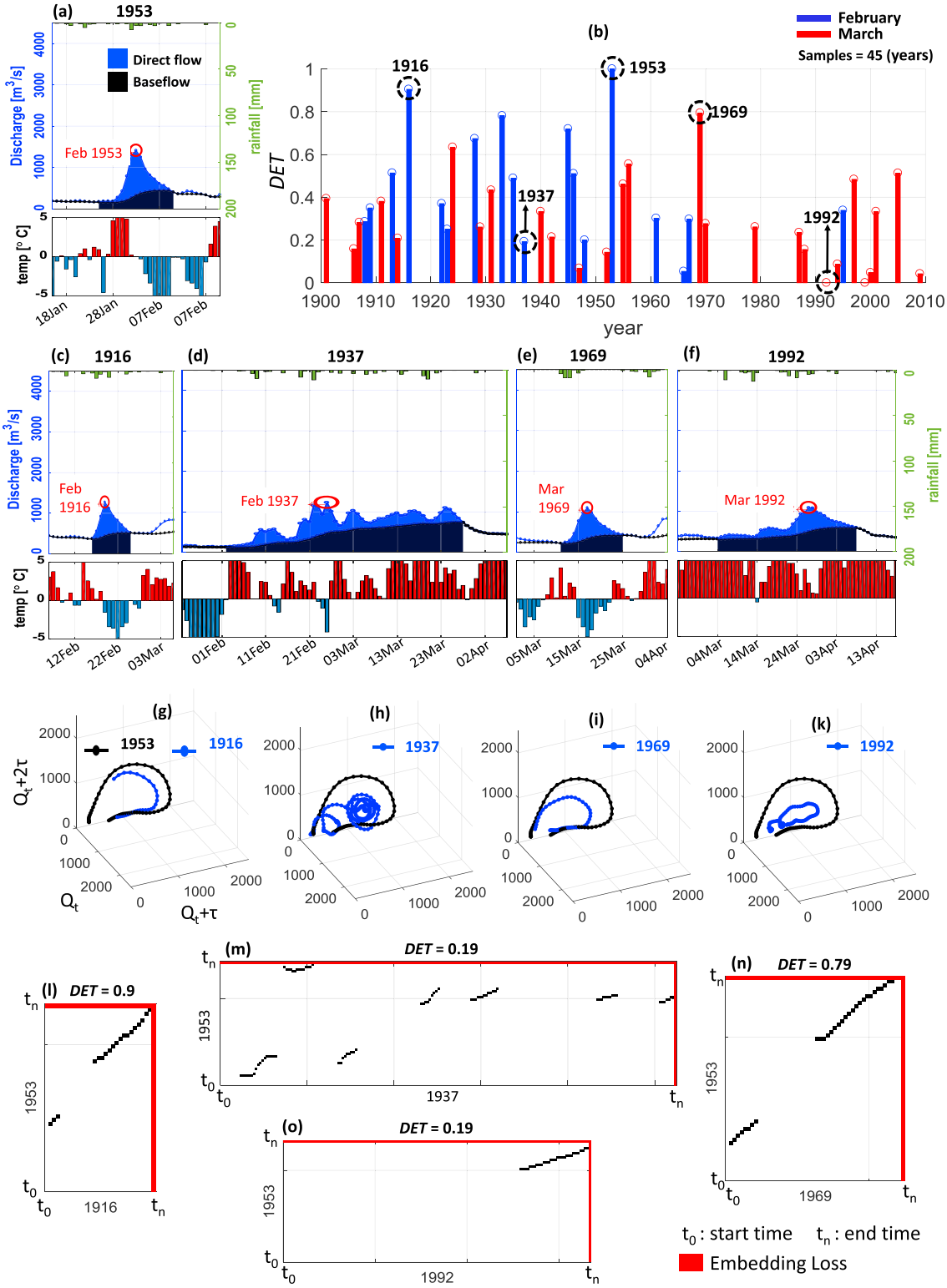

Figure 8. Comparing the February 1953 event to all other annual maxima that occurred in February and March. (a) Reference hydrograph 1953; (b) *DET* values resulting from the pairwise comparison; (c and e) example hydrographs with high *DET* values; (d and f) example hydrographs with low *DET* values; (g–k) phase space trajectories of the example hydrographs and the 1953 event; (l–o) CRP plots comparing 1953 to the example hydrographs. Note that the CRP grid are plotted with equal *x* and *y* tick axis distance of 10 days.

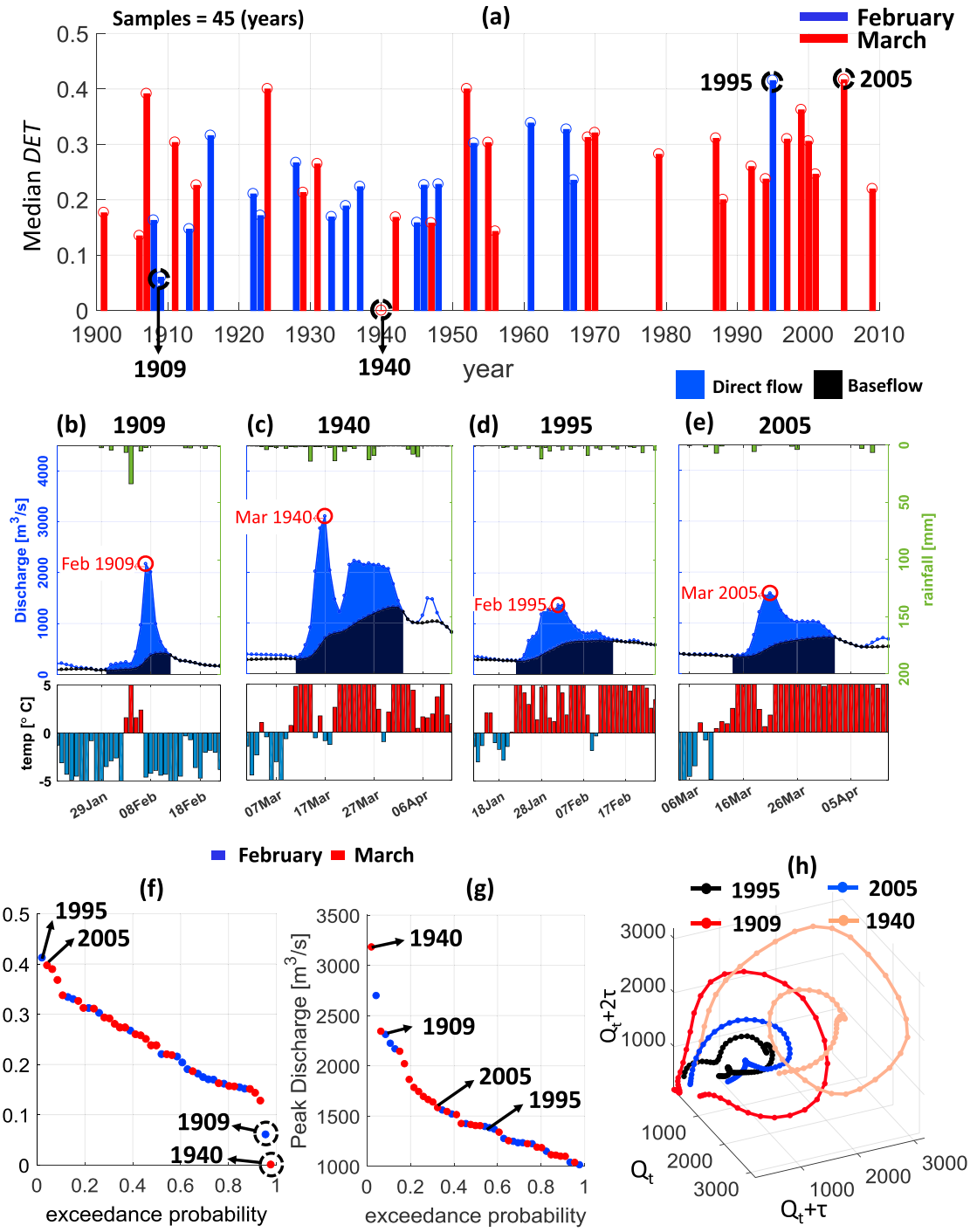

Figure 9. Intercomparison of all February and March flood hydrographs: (a) median *DET* values; (b and c) hydrographs of the two events with the lowest median *DET* values; (d and e) hydrographs of the two events with the highest *DET* values; (f and g) empirical distribution of peak discharge and median *DET* values; and (h) phase space trajectories for the events with the two highest and lowest median *DET* values.

hydrograph shape suggests that, by the time of the second peak, the ice debris had accumulated and jammed the river, so that the high flood water level of the river was kept constant for an unusually long duration.

The 1909 flood (Figure 9b) has the second lowest median *DET* value and the fourth highest peak discharge. This event was also recorded in the archive as unusual; very heavy rain was combined with icy and deep frozen ground (Röttcher & Deutsch, 2009; Schuh, 2011). The rainfall intensity was unusually high for this season; such high intensities are rather observed in the summer season in the Elbe catchment (Petrow et al.,

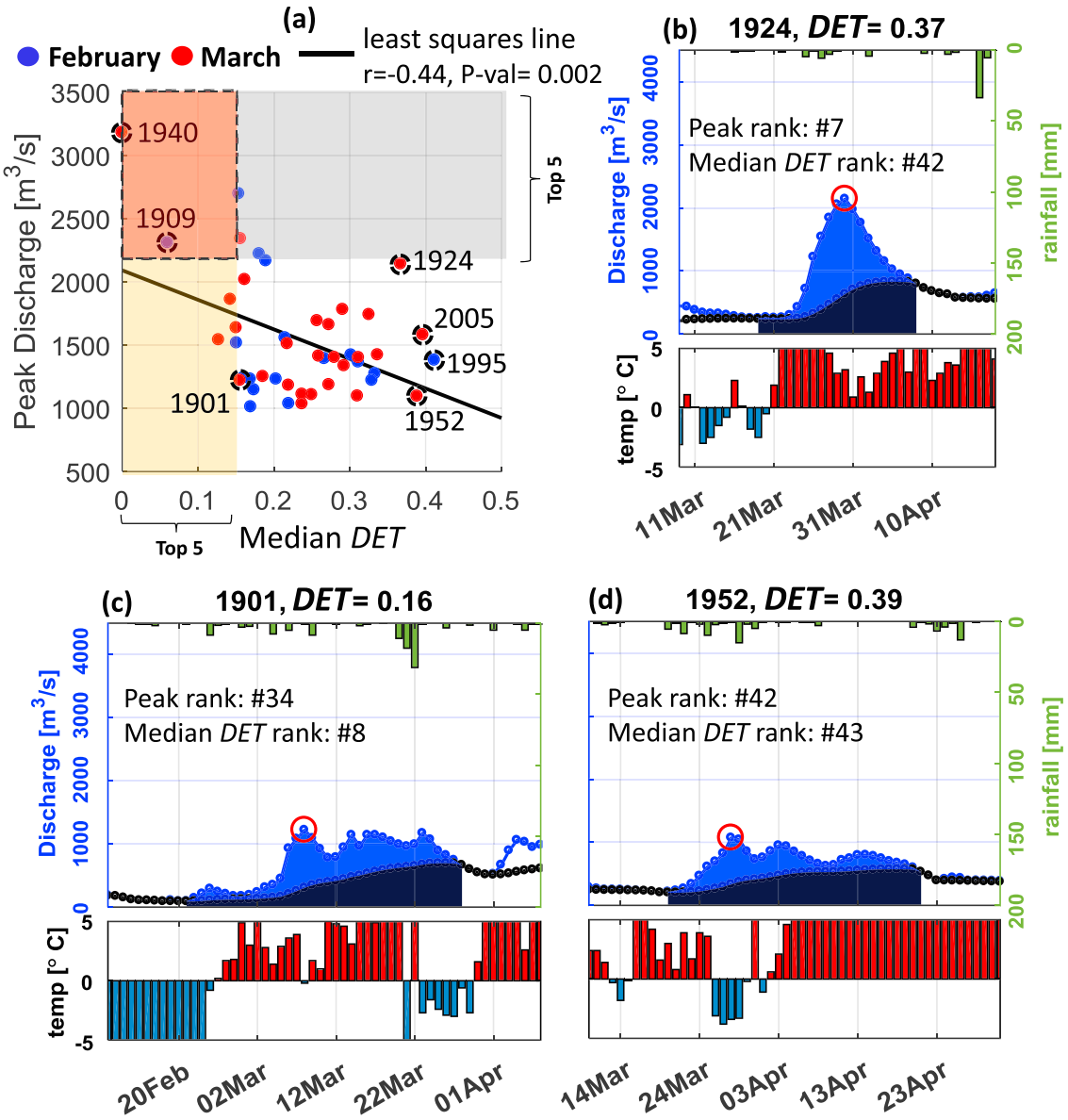

Figure 10. Relationship between flood peak discharge and median *DET* (a) with each top 5 of the index being shaded (gray, high discharge; yellow, low values of median *DET*; orange, overlap of both top 5). Three further examples of event hydrographs with common (b and d) and rare (c) runoff dynamics.

2007). The superposition of intensive rainfall with frozen ground led to an exceptionally peakish hydrograph shape with steep rising and falling slope. Interestingly, the antecedent catchment conditions were rather dry. The streamflow at the event start was 90 m^3/s, while the median of all annual maximal floods in February and March is 200 m^3/s. This event was caused by different flood generation processes compared to the typical rain-on-snow floods (Merz & Blöschl, 2003) in February and March at the gauge Dresden, where snowmelt prior or during the flood event increases the catchment wetness and amplifies the impact of moderate rainfall (Nied et al., 2017).

The floods in 1995 and 2005 (Figures 9d and 9e) have the highest median *DET* values, which suggests that these events represent the most common flood runoff dynamics. Their hydrographs show a rather prolonged recession. Figure 9h compares the phase space trajectories of these four events. The events in 1995 and 2005 are rather similar to each other, while the events in 1909 and 1940 with the lowest median *DET* values have very different trajectories.

The two events with the lowest median *DET* value have the highest and fourth highest peak discharge. This could suggest a link between unusual runoff dynamics and extreme discharge in the sense that the extremes are generated by different processes compared to the majority of floods. Figure 10a plots peak discharge versus median *DET* values. There is a moderate correlation (Pearson correlation coefficient $r = -0.44$), significant at the 1% level. Hence, there is a tendency that floods with extreme peak discharges have unusual runoff dynamics as shown by the floods 1940 and 1909, which are both within the top 5 of the indices (shaded orange), and that moderate or low peaks have rather common runoff dynamics (e.g., floods 2005 and 1995). However, not all events with extreme peaks are characterized by rare runoff dynamics and vice versa. For instance, the 1924 flood has a considerable peak discharge above 2,000 m^3/s (peak discharge rank 7) but a common hydrograph shape (median *DET* rank 42), while the 1901 event with low peak discharge (peak discharge rank 34) shows a rather unusual runoff dynamics (median *DET* rank 8) with five peaks and unusual fluctuations within the event. Multiple peaks are not necessarily unusual; for instance, the event 1952 has a rather common hydrograph with three subevents that are smooth in their transition (median *DET* rank 43).

To further assess the proposed CRP-based measure against frequently used hydrological signatures, we compare it against the baseflow index, the rising and falling slope, and the volume and duration of the hydrograph. The rising and falling slope ΔQ_{rise} and ΔQ_{fall} are calculated as the gradient during the flood event prior to the peak (i.e., from the start of the event to the peak) and after the peak (i.e., from the peak to the end of the event), respectively. The volume V is calculated as an approximate integral of the total discharge using the trapezoidal method, and the baseflow index BFI is the ratio of baseflow and total discharge volume, also derived using the same integral approximation.

We plot each signature against the median *DET* value for the flood event set (Figure 11) and measure its correlation using the Pearson correlation coefficient R. Falling slope and baseflow index show a positive correlation, significant at the 1% level, that is, events with rare runoff dynamics show steeper recessions and a lower fraction of baseflow. This result can be explained by the dominant flood generation processes. Floods in February and March are typically snowmelt events or rain-on-snow events with moderate to low rainfall leading to slow recessions. Hence, events with mild falling slopes are not considered as rare or unusual. These dominant flood types also explain the relation between BFI and median *DET*. Winter floods are often characterized by a high fraction of baseflow. The remaining signatures do not show a significant relation with median *DET*.

Table 1 compares the top 5 events for each index. For visual comparison, all hydrographs can be found in Figure C1 in the appendix. The most unusual event identified by the CRP-based measure, the 1940 flood, is also unusual in terms of high peak discharge, steep rising slope, and high volume. Although its shape is clearly an outlier with a steep first peak and a second peak, which is held constant for 10 days due to ice blocking the river, the falling slope index does not suggest that this event is unusual, since both slopes are aggregated into one value hiding the very specific event characteristics. The second and fourth unusual events, the floods in 1909 and 1956, are set apart from the other events by their unusually steep rising and falling slopes and low baseflow index. The third unusual event, the 1906 flood, is not within the top 5 events of any of the hydrological signatures. In terms of these signatures, this event is not particularly unusual. However, it has indeed an unsual shape with a long upfront limb with comparatively low variability. The 1942 event, the fifth unusual flood, is also characterized as particular by the volume and duration.

The comparison of the CRP-based similarity measure with the conventional hydrological signatures shows that it characterizes different events as unusual. It shows moderate correlation with the falling slope, baseflow index, and peak discharge, but no significant relation to the other signatures. These differences can be explained by the different conceptual approaches: *DET* quantifies the event runoff dynamics by taking into account the temporal evolution of the discharge values of the entire event. In contrast, the conventional hydrograph signatures consider either one specific component of the hydrograph or are an aggregated value. Hence, they provide a less comprehensive picture, as they either focus on a specific component or lump across several characteristics, such as the slope averaged across several subevents. It is interesting to note that the proposed CRP-based measure does not only characterize events with very particular hydrograph shapes as unsual, such as the double-peak 1940 flood where the second peak is almost constant for 10 days due to ice blocking the river. It also detects events that have a common single-peak shape but are unusual in terms of low baseflow and steep slopes, such as the 1909 event. An advantage of the hydrological signa-

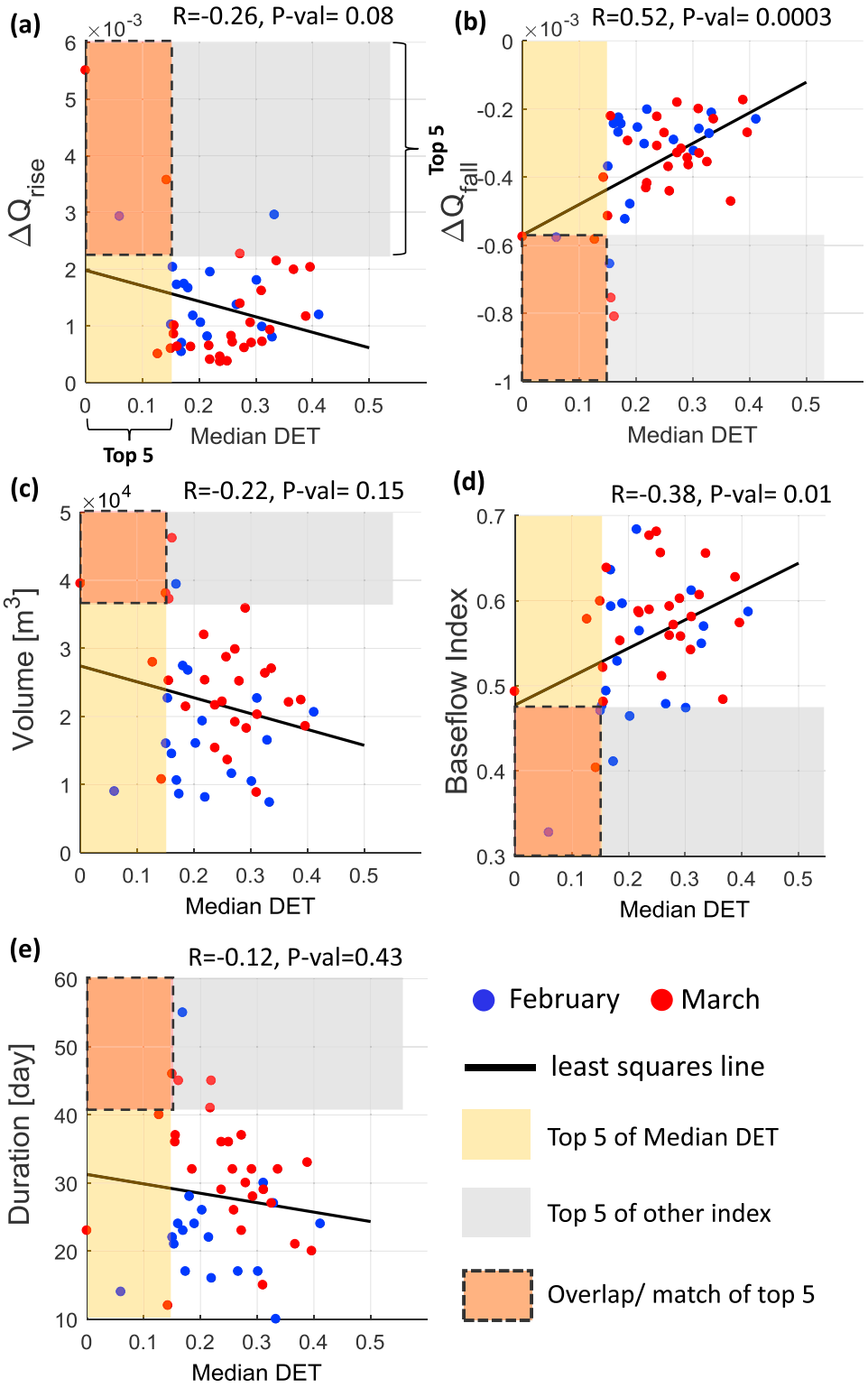

Figure 11. Scatterplots of hydrological signatures versus median *DET*: (a) rising slope ΔQ_{rise}, (b) falling slope ΔQ_{fall}, (c) event volume, (d) baseflow index BFI, and (e) event duration. The shaded areas show the top 5 events for each signature index. In addition, the Pearson correlation coefficient *R* and the *P* value are given.

Table 1
Top 5 Most Unusual Events in Terms of Median DET and Different Hydrological Signatures

No.	Index	1st	2nd	3rd	4th	5th	Exact match	Match diff. rank	Total match
1	Median *DET* – lowest	1940	1909	1906	1956	1942			
2	Peak discharge – highest	1940	1923	1947	1909	1946	1	1	2
3	Rising slope (ΔQ_{rise}) – steepest	1940	1956	1909	1916	1923	1	2	3
4	Falling slope (ΔQ_{fall}) – steepest	1909	1923	1956	1931	1948	—	2	2
5	Volume – highest	1988	1940	1937	1942	1947	—	2	2
6	Baseflow index – lowest	1909	1956	1933	1922	1945	—	2	2
7	Duration – longest	1937	1942	1988	2009	1914	—	1	1

Note. The last three columns show the match between median *DET* and the hydrological signatures.

tures is that they provide an explanation why they characterize an event as unusual. However, due to their specific nature, several signatures need to be considered jointly to judge whether a hydrograph is unusual.

To compare our approach with a well-established method, we utilize these signatures as a joint index to identify rare events through clustering. We use hierarchical clustering with the euclidean distance as classification factor. Each signature is normalized before the clustering. Figure 12a shows a of the three main event clusters and the five outliers of the three main event clusters and the five outliers. Their variation across the hydrological signatures is given in Figure 12b. The outliers 1 (1940), 2 (1909), and 3 (1956) are characterized by high rising slope ΔQ_{rise} and also moderate to high discharge peak, while outliers 4 (1988) and 5 (1937) are associated with high baseflow index, long duration, and overall volume. With reference to the events' median DET, three of these outliers are within the lowest five, except events 1988 and 1937 with median *DET* are ranked 11th and 12th, respectively.

Despite the close characteristics of these 1988 and 1937 events from their conventional signatures and hence combined into a cluster, their hydrographs look visibly dissimilar. The reason of such misleading similarity assessment lies on the calculation of certain index instead of and prior to the clustering method. For instance ΔQ_{rise}, where the existence of several subevents and hence variation of magnitudes before the flood peak enlarge the uncertainty of the slope value, as these varying values are averaged by a linear slope of single line drawn from the starts of events to their peaks. In contrast, the CRPs between these two hydrographs show hardly any clear diagonal lines and very low *DET* value indicating dissimilarity (see Figure 13).

4. Conclusions

Based on the concept of RPs, we propose a novel hydrograph similarity measure. The event runoff dynamics is characterized by its continuous time sequence; that is, the entire hydrograph shape is represented as phase space trajectory. Since the phase space vector is reconstructed using multidimensional time delay embedding, each point of the phase space trajectory contains the relation of several points in time within the event hydrograph, including, for example, the initial flow conditions caused by antecedent rainfall. The phase space vectors of two events are then analyzed and compared directly for their similarity using CRPs instead of being summarized as an index first before comparison. Thereafter, the resulted CRPs are summarized using one of the RQA measures called determinism (*DET*).

The closest concept to this similarity assessment using CRP and *DET* is a scatter plot between two time series and its correlation coefficient. The comparison between these two concepts demonstrates the benefit of the proposed method. In contrast to scatter plots and correlation analysis, the CRP-based method allows comparing time series of different duration, and it detects similar or identical signals that are shifted in time. In contrast to correlation analysis, CRP is not limited to monotonic, linear relations and the time when similar patterns occur, that is, as long as both trajectories are common. The most important benefit stems, however, from the fundamentally different approach of the CRP-based method to quantify similarity based on the multidimensional relation of different magnitudes in time within an event.

We further provide recommendations how to parameterize CRP. This includes the adaptation of a method recently proposed by Wendi and Marwan (2018) to properly select the time delay and embedding dimension to prevent artifacts in the analysis. This suggests the use of measure called *DET* distance to evaluate

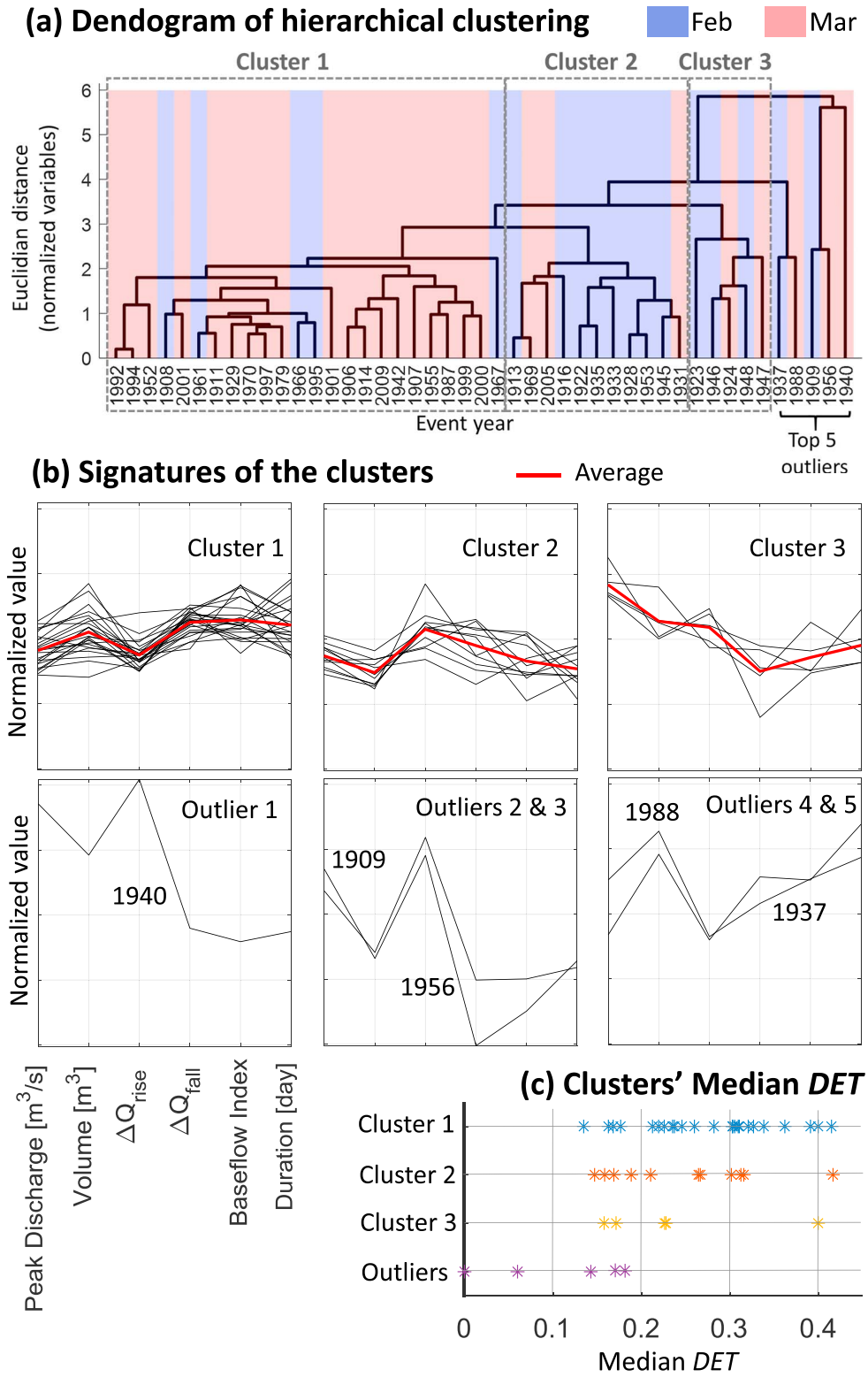

Figure 12. Clusters of events characteristics by considering the joint indices of their conventional signatures through hierarchical clustering method with euclidean distance. (a) Dendogram of the clusters and the top 5 outliers, (b) signatures of each cluster and outlier, (c) median *DET* values of the clusters and outliers.

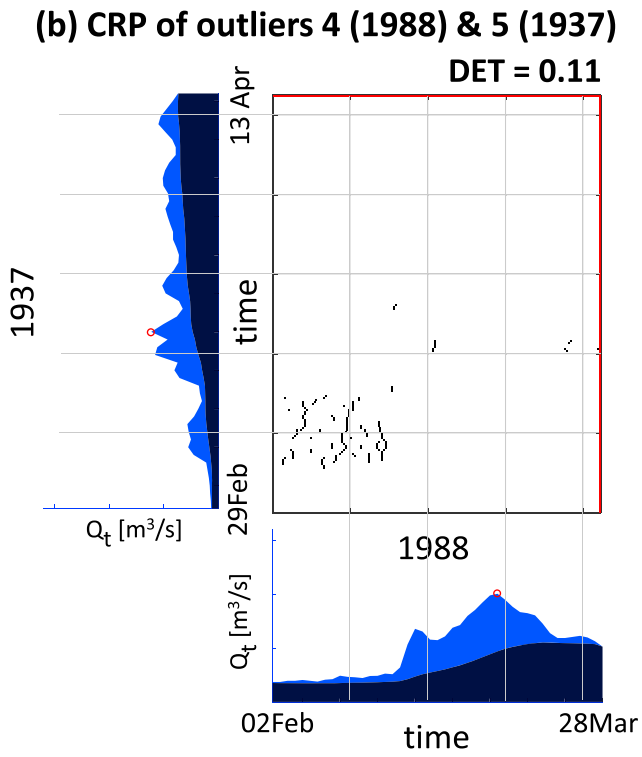

Figure 13. Cross recurrence plot (CRP) between the cluster of outliers 4 (year 1988) and 5 (year 1937).

the safety of an embedding parameter set within an acceptable embedding loss (i.e., ≤10% of hydrograph length). The choice of embedding dimension (m) can be subjective as well to the user's requirements, such as how complex should each vector in the phase space represent, for example, to include the implications of a minimum number of antecedents conditions. For instance, a vector in a four-dimensional phase space can describe the relationship between flood peak discharge and three other prior discharge values, that is, at τ, 2τ, and 3τ earlier. From our experience with the application example, we noticed that hydrographs with longer durations and multipeaks generally require higher embedding dimension to attain maximum *DET* distance. We also suggest the use of the local minima method with a phase distance threshold (Schultz et al., 2011; Wendi & Marwan, 2018) to define the recurrence points for a more robust CRP, that is, which is less dependent on the threshold ϵ and avoid thick lines artifacts.

In the application example, we show that through intercomparing every flood hydrograph in a pairwise manner, we can evaluate whether an event is unusual in terms of its runoff dynamics as assessed using median values of their *DET*s. Interestingly, the two floods with the lowest median *DET*, suggesting the most unusual runoff dynamics, are events that are also described as unusual in the historical archives in terms of their flood generation processes. The double-peak 1940 flood contains an almost constant second peak for several days caused by blockage of the river due to ice debris. The second most unusual event, the 1909 flood, was caused by the superposition of very heavy rainfall on frozen ground. This rainfall can be described as unseasonal, as such high intensities are unusual in this season in the study catchment.

The comparison of the proposed hydrograph similarity measure with conventional hydrological signatures individually shows that each measure defines different events as unusual. This was expected as each measures puts the focus on different aspects when measuring similarity. The conventional hydrological signatures focus on particular components of the hydrograph or lump characteristics into an aggregate value. This provides a partial quantification of similarity only and may lead to wrong conclusions, for instance, by hiding specific hydrograph characteristics through the aggregation. Further, our example shows that multivariate indices, which combine several hydrological signatures, can still misidentify similar hydrographs. The cause of this misidentification is the aggregation into a single value before the comparison. Since the proposed measure compares phase space trajectories that build on time delay embedding and, hence, directly

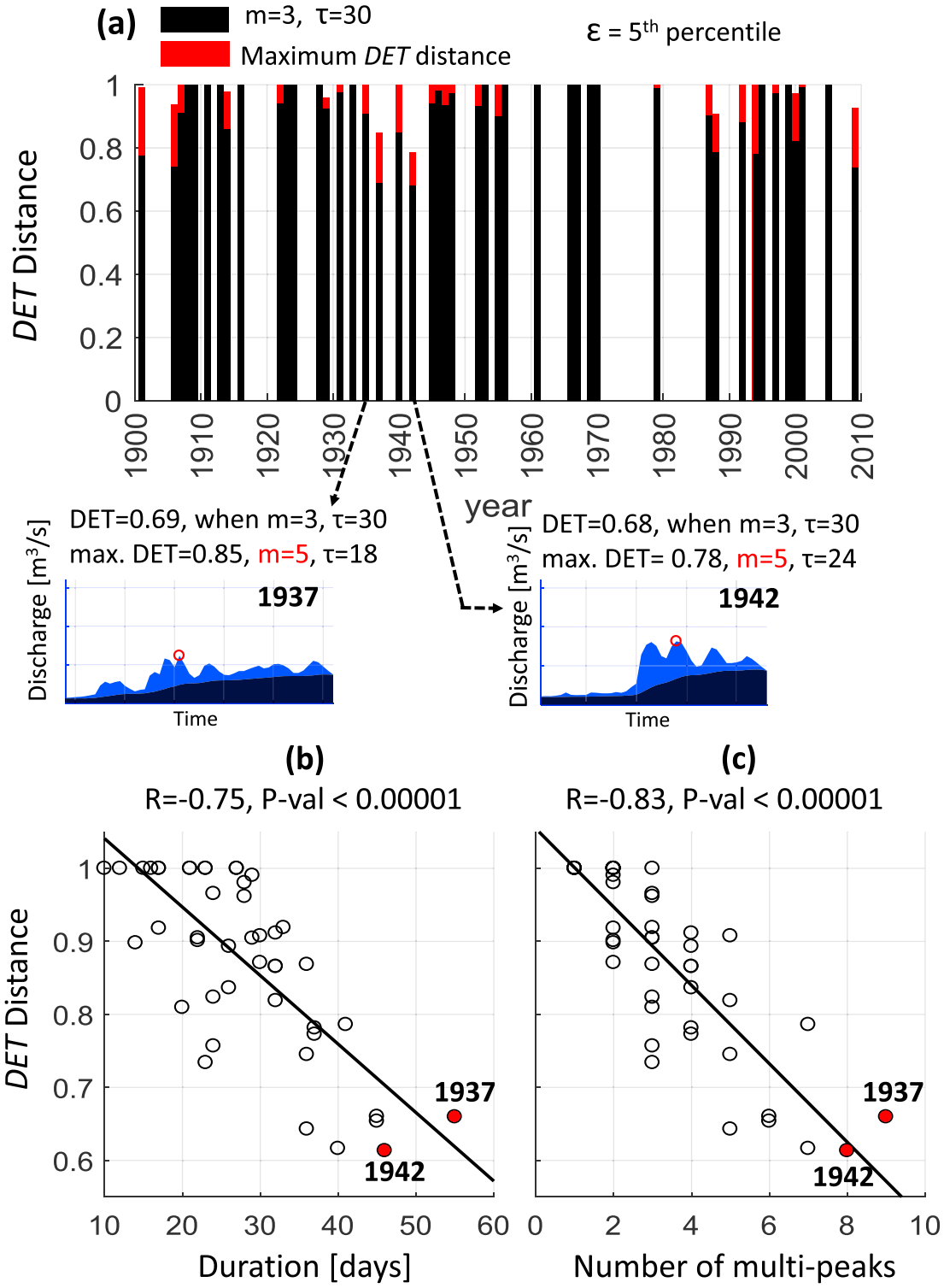

Figure A1. Parameters evaluation for all events: (a) *DET* distances of all events based on the selected parameters set of $m = 3$ and $\tau = 30$ hr (black bar), and maximum *DET* distances from possible sets of parameters within $1 \leq m \leq 10$ and $6 \leq \tau \leq 60$ hr. Examples are shown for event 1937 and 1942 where its maximum *DET* distance can be achieved by using higher m; (b) and (c) are scatter plots and correlations between *DET* distance and event duration and number of multipeaks in the hydrographs.

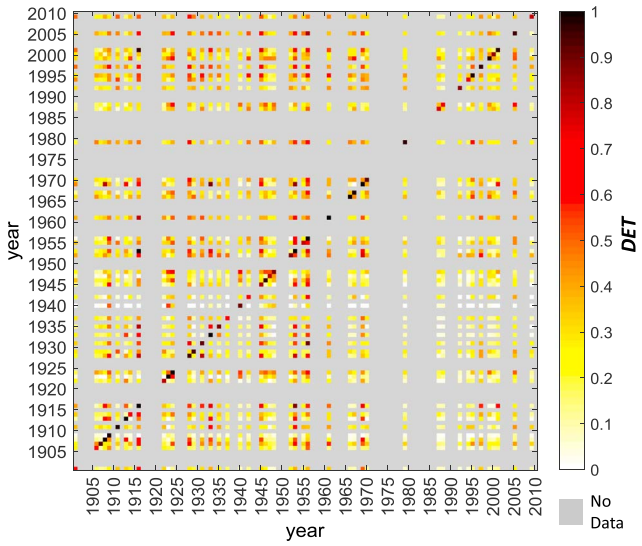

Figure B1. *DET* Matrix of all pairwise flood hydrographs in February and March extracted from Dresden station from 1901 to 2010. Gray indicates no event satisfied the selection criteria.

compares the entire set of hydrograph magnitudes and their unique time sequence, we argue that it provides a more comprehensive similarity measure.

However, when working with real world observations, the presence of noise might cause the diagonal in CRP to be discontinuous and hence decreases the *DET* values or herein used as similarity index. Therefore, if noise presence is known to be prominent, user should consider noise reduction of the signal before conducting CRP analysis. In addition, unlike the comparison of using commonly signatures, the similarity index DET does not easily provide intuitive and specific meaning to the similarity found in the hydrograph. Besides, reference in the application of hydrology is not yet available.

To our knowledge, this is the first application of (Cross) Recurrence Plots and RQA in catchment hydrology. We project these methods have a large application potential in hydrology. A straightforward extension would be to analyze longer periods, such as annual or seasonal hydrographs instead of just events, in order to evaluate if there has been a change in the hydrological regime over time. These methods could also be used to calibrate and validate hydrological and hydrodynamic simulation models, by applying them as measure to quantify the agreement between simulation results and observations.

Appendix A: Parameter Evaluation for All Events Using *DET* Distance

Figure A1 shows the parameter set evaluations of all events through *DET* distance with both the selected set of $m = 3$ and $\tau = 30$ hr and sets that allow maximum *DET* distance. Two events with the lowest *DET* distances were identified to have the hydrographs with longest duration and highest number of multipeaks. For these two events to result in higher *DET* distance, higher embedding dimension m with different *tau* are required. In general events hydrographs with longer duration that contains more multipeaks tend to have lower *DET* distance and therefore would require a higher m.

Appendix B: *DET* Matrix of All Pairwise Flood Hydrographs

Figure B1 shows the *DET* Matrix of all pairwise flood hydrographs that is used for median *DET* summary.

Appendix C: Extracted Hydrographs in Dresden Station

Figure C1 contains all the extracted hydrographs sorted based on their median *DET* values (from low that indicates rare runoff dynamics to high that indicates common runoff dynamics).

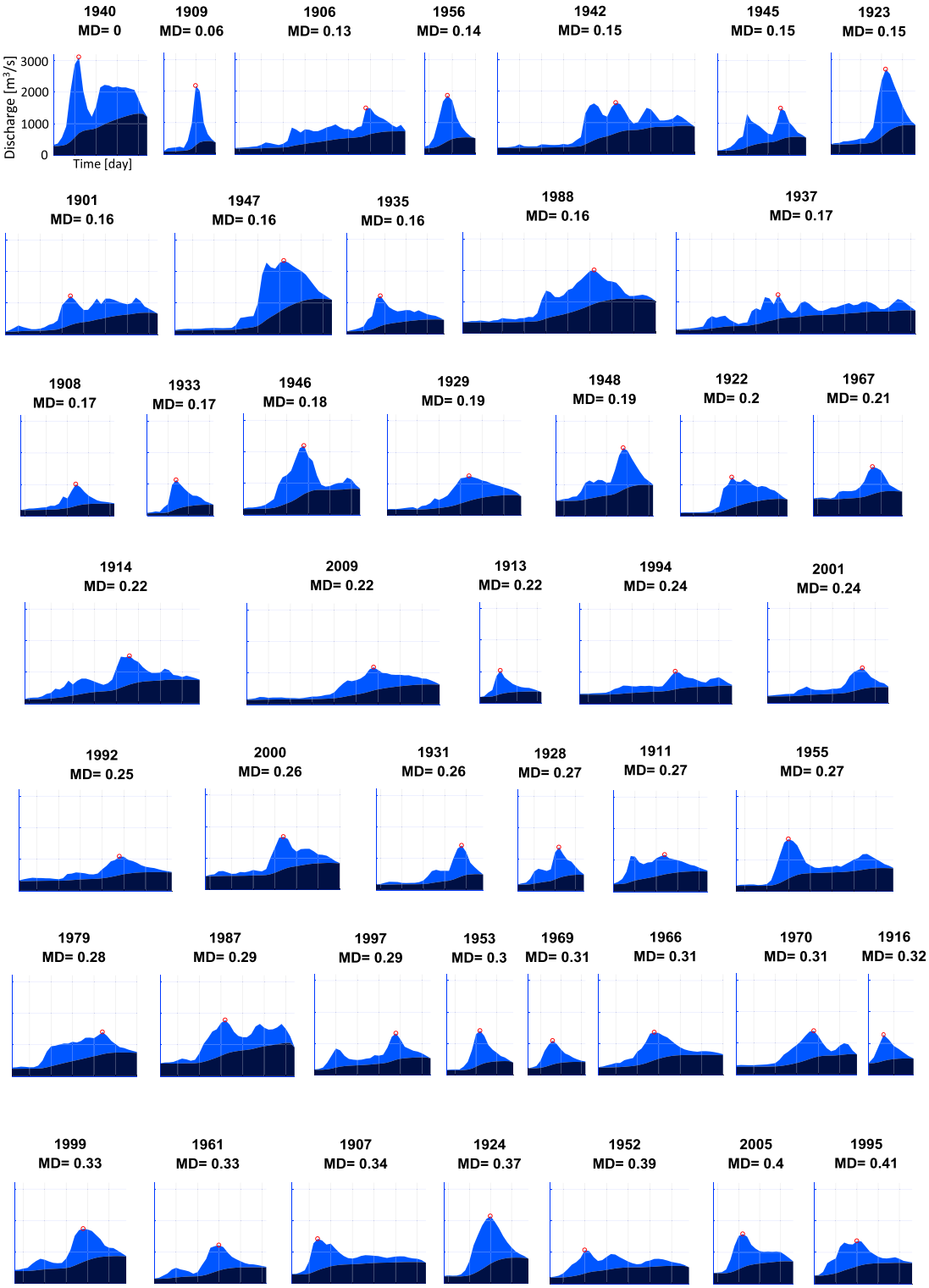

Figure C1. Hydrographs of all selected February and March floods sorted by median *DET* (MD). Smaller MD values characterize more unusual events in terms of runoff dynamics.

Acknowledgments
This research was carried out within the Research Training Group "Natural Hazards and Risks in a Changing World" (NatRiskChange; GRK 2043/1) funded by the Deutsche Forschungsgemeinschaft (DFG). We would also like to acknowledge and thank for the Dresden discharge data provided by the Federal Institute for Hydrology (BfG).

References

Aceves-Fernandez., M. A., Ramos-Arreguín, J. M., Pedraza-Ortega, J. C., Sotomayor-Olmedo., A., & Tovar-Arriaga, S. (2012). Finding trends of airborne harmful pollutants by using recurrence quantification analysis. *American Journal of Environmental Engineering*, *1*(1), 10–14. Retrieved from https://doi.org/10.5923/j.ajee.20110101.02

Bárdossy, A. (2006). Calibration of hydrological model parameters for ungauged catchments. *Hydrology and Earth System Sciences*, *3*(3), 1105–1124. Retrieved from https://doi.org/10.5194/hess-11-703-2007

Blöschl, G., Sivapalan, M., Wagener, T., Viglione, A., & Savenije, H. (2011). Prediction of floods in ungauged basins, *Runoff prediction in ungauged basins: Synthesis across processes, places and scales* (pp. 189–225). Cambridge: Cambridge University Press. Retrieved from http://ebooks.cambridge.org/ref/id/CBO9781139235761 https://doi.org/10.1017/CBO9781139235761

Boughton, W. C. (1993). *A hydrograph-based model for estimating the water yield of ungauged catchments*. In Proceedings of the 1993 Hydrology and Water Resources Symposium, Institution of Engineers, Australia, National Conference Publication 93/14, 317–324.

Brunner, M. I., Viviroli, D., Sikorska, A. E., Vannier, O., Favre, A.-C., & Seibert, J. (2017). Flood type specific construction of synthetic design hydrographs. *Water Resources Research*, *53*, 1390–1406. Retrieved from https://doi.org/10.1002/2016WR019535

Carrubba, S., Frilot, C., Chesson, A. L., & Marino, A. A. (2010). Mobile-phone pulse triggers evoked potentials. *Neuroscience Letters*, *469*(1), 164–168. Retrieved from https://doi.org/10.1016/J.NEULET.2009.11.068

Crowley, P. M. (2008). Analyzing convergence and synchronicity of business and growth cycles in the euro area using cross recurrence plots. *European Physical Journal – Special Topics*, *164*(1), 67–84. https://doi.org/10.1140/epjst/e2008-00835-3

Eckmann, J.-P., Oliffson Kamphorst, S., Ruelle, D., Kamphorst, S. O., & Ruelle, D. (1987). Recurrence plots of dynamical systems. *EPL (Europhysics Letters)*, *4*(9), 973. Retrieved from https://stacks.iop.org/0295-5075/4/i=9/a=004http://iopscience.iop.org/0295-5075/4/9/004

Ehret, U., & Zehe, E. (2011). Series distance an intuitive metric to quantify hydrograph similarity in terms of occurrence, amplitude and timing of hydrological events. *Hydrology and Earth System Sciences*, *15*(3), 877–896. Retrieved from https://doi.org/10.5194/hess-15-877-2011

Elshorbagy, A., Simonovic, S. P., & Panu, U. S. (2002). Noise reduction in chaotic hydrologic time series: Facts and doubts. *Journal of Hydrology*, *256*(3-4), 147–165. Retrieved from https://www.sciencedirect.com/science/article/pii/S0022169401005340, https://doi.org/10.1016/S0022-1694(01)00534-0

Eroglu, D., McRobie, F. H., Ozken, I., Stemler, T., Wyrwoll, K.-H., Breitenbach, S. F. M., et al. (2016). Seesaw relationship of the Holocene East AsianâĂŞAustralian summer monsoon. *Nature Communications*, *7*, 12929. Retrieved from http://www.nature.com/doifinder/10.1038/ncomms12929, https://doi.org/10.1038/ncomms12929

Fraser, A. M., & Swinney, H. L. (1986). Independent coordinates for strange attractors from mutual information. *Physical Review A*, *33*(2), 1134–1140. Retrieved from http://link.aps.org/doi/10.1103/PhysRevA.33.1134, https://doi.org/10.1103/PhysRevA.33.1134

Goswami, B., Boers, N., Rheinwalt, A., Marwan, N., Heitzig, J., Breitenbach, S. F. M., & Kurths, J. (2018). Abrupt transitions in time series with uncertainties. *Nature Communications*, *9*(1), 48. Retrieved from http://www.nature.com/articles/s41467-017-02456-6, https://doi.org/10.1038/s41467-017-02456-6

Haaf, E., & Barthel, R. (2018). An inter-comparison of similarity-based methods for organisation and classification of groundwater hydrographs. *Journal of Hydrology*, *559*, 222–237. Retrieved from http://www.sciencedirect.com/science/article/pii/S0022169418301112#b0075, https://doi.org/10.1016/J.JHYDROL.2018.02.035

Hannah, D. M., Smith, B. P. G., Gurnell, A. M., & McGregor, G. R. (2000). An approach to hydrograph classification. *Hydrological Processes*, *14*(2), 317–338. https://doi.org/10.1002/(SICI)1099-1085(20000215)14:2<317::AID-HYP929>3.0.CO;2-T

Hattermann, F. F., Huang, S., Burghoff, O., Willems, W., Österle, H., Büchner, M., & Kundzewicz, Z. (2014). Modelling flood damages under climate change conditions a case study for Germany. *Natural Hazards and Earth System Sciences*, *14*, 3151–3169. Retrieved from http://www.nat-hazards-earth-syst-sci.net/14/3151/2014/, https://doi.org/10.5194/nhess-14-3151-2014

Hrachowitz, M., Savenije, H. H. G., Blöschl, G., Mcdonnell, J. J., Sivapalan, M., Pomeroy, J. W., et al. (2013). A decade of Predictions in Ungauged Basins (PUB)—A review. *Hydrological Sciences Journal*, *58*(6), 1198–1255. Retrieved from http://www.tandfonline.com/action/journalInformation?journalCode=thsj20%, https://doi.org/10.1080/02626667.2013.803183

Kantz, H., & Schreiber, T. (2005). Nonlinear time series analysis. *Technometrics*, *47*(3), 381–381. Retrieved from https://doi.org/10.1198/tech.2005.s306

Kennel, M. B., Brown, R., & Abarbanel, H. D. I. (1992). Determining embedding dimension for phase-space reconstruction using a geometrical construction. *Physical Review A*, *45*(6), 3403–3411. Retrieved from https://doi.org/10.1103/PhysRevA.45.3403

Krämer, K. H., Donner, R. V., Heitzig, J., & Marwan, N. (2018). Recurrence threshold selection for obtaining robust recurrence characteristics in different embedding dimensions. *Chaos*, *28*(8), 085720. https://doi.org/10.1063/1.5024914

Marwan, N. (2010). How to avoid potential pitfalls in recurrence plot based data analysis. *International Journal of Bifurcation and Chaos*, *21*(04), 1003–1017. Retrieved from https://doi.org/10.1142/S0218127411029008

Marwan, N., Carmen Romano, M., Thiel, M., & Kurths, J. (2007). Recurrence plots for the analysis of complex systems. *Physics Reports*, *438*(5-6), 237–329. Retrieved from https://doi.org/10.1016/j.physrep.2006.11.001

Marwan, N., & Meinke, A. (2004). Extended recurrence plot analysis and its application to ERP data. *International Journal of Bifurcation and Chaos*, *14*(2), 761–771.

Marwan, N., Thiel, M., & Nowaczyk, N. R. (2002). Cross recurrence plot based synchronization of time series. *Nonlinear Processes in Geophysics*, *9*(3/4), 325–331. Retrieved from https://doi.org/10.5194/npg-9-325-2002

Marwan, N., Wessel, N., Meyerfeldt, U., Schirdewan, A., & Kurths, J. (2002). Recurrence plot based measures of complexity and its application to heart rate variability data. *Physical Review E*, *66*(2), 26702. https://doi.org/10.1103/PhysRevE.66.026702

Matti, B., Dahlke, H. E., Dieppois, B., Lawler, D. M., & Lyon, S. W. (2017). Flood seasonality across Scandinavia—Evidence of a shifting hydrograph? *Hydrological Processes*, *31*, 4354–4370. Retrieved from https://doi.org/10.1002/hyp.11365

Merz, R., & Blöschl, G. (2003). A process typology of regional floods. *Water Resources Research*, *39*(12), 1340. Retrieved from https://doi.org/10.1029/2002WR001952

Nied, M., Schröter, K., Lüdtke, S., Nguyen, V. D., & Merz, B. (2017). What are the hydro-meteorological controls on flood characteristics? *Journal of Hydrology*, *545*, 310–326. Retrieved from https://doi.org/10.1016/J.JHYDROL.2016.12.003

Oberst, S., & Lai, J. C. S. (2015). Nonlinear transient and chaotic interactions in disc brake squeal. *Journal of Sound and Vibration*, *342*, 272–289. https://doi.org/10.1016/j.jsv.2015.01.005

Packard, N. H., Crutchfield, J. P., Farmer, J. D., & Shaw, R. S. (1980). Geometry from a time series. *Physical Review Letters*, *45*(9), 712–716. Retrieved from https://doi.org/10.1103/PhysRevLett.45.712

Peel, M. C., & Blöschl, G. (2011). Hydrological modelling in a changing world. *Progress in Physical Geography*, *35*(2), 249–261. Retrieved from https://doi.org/10.1177/0309133311402550

Petrow, T., Merz, B., Lindenschmidt, K.-E., & Thieken, A. H. (2007). Aspects of seasonality and flood generating circulation patterns in a mountainous catchment in south-eastern Germany. *Hydrology and Earth System Sciences*, *11*(4), 1455–1468. Retrieved from https://doi.org/10.5194/hess-11-1455-2007

Röttcher, K., & Deutsch, M. (2009). 100 Jahre Hochwasser 1909 Was interessiert uns das heute noch?Zeitschrift: WasserWirtschaft, 42/ 43.

Sawicz, K. A., Kelleher, C., Wagener, T., Troch, P., Sivapalan, M., & Carrillo, G. (2014). Characterizing hydrologic change through catchment classification. *Hydrology and Earth System Sciences*, *18*(1), 273–285. Retrieved from https://hydrol-earth-syst-sci.net/18/273/2014/, https://doi.org/10.5194/hess-18-273-2014

Schuh, A. (2011). Eishochwasser an Oder und Elbe aus historischen und meteorologischen Gesichtspunkten und im Hinblick auf mögliche Gefährdungen (Doctoral dissertation), Brandenburgischen Technischen Universität Cottbus. Retrieved from https://opus4.kobv.de/opus4-btu/frontdoor/index/index/docId/2274

Schultz, A. P., Zou, Y., Marwan, N., & Turvey, M. T. (2011). Local minima-based recurrence plots for continuous dynamical systems. *International Journal of Bifurcation and Chaos*, *21*(04), 1065–1075. Retrieved from https://doi.org/10.1142/S0218127411029045

Sivakumar, B. (2000). Chaos theory in hydrology: Important issues and interpretations. *Journal of Hydrology*, *227*(1), 1–20. Retrieved from https://doi.org/10.1016/S0022-1694(99)00186-9

Takens, F. (1981). Detecting strange attractors in turbulence. In D. Rand & L. S. Young (Eds.), *Dynamical systems and turbulence, Warwick 1980*, Lecture Notes in Mathematics (Vol. 898). Berlin, Heidelberg: Springer. Retrieved from https://doi.org/10.1007/BFb0091924

Ternynck, C., Ben Alaya, M. A., Chebana, F., Dabo-Niang, S., Ouarda, TahaB. M. J., Ternynck, C., et al. (2016). Streamflow hydrograph classification using functional data analysis. *Journal of Hydrometeorology*, *17*(1), 327–344. Retrieved from https://doi.org/10.1175/JHM-D-14-0200.1

Trulla, L. L., Giuliani, A., Zbilut, J. P., & Webber, C. L. (1996). Recurrence quantification analysis of the logistic equation with transients. *Physics Letters, Section A: General, Atomic and Solid State Physics*, *223*(4), 255–260. Retrieved from https://doi.org/10.1016/S0375-9601(96)00741-4

Wendi, D., & Marwan, N. (2018). Extended recurrence plot and quantification for noisy continuous dynamical systems. *Chaos*, *28*(8), 085722. Retrieved from https://doi.org/10.1063/1.5025485

Wendi, D., Marwan, N., & Merz, B. (2018). In search of determinism-sensitive region to avoid artefacts in recurrence plots. *International Journal of Bifurcation and Chaos*, *28*(01), 1850007. Retrieved from https://doi.org/10.1142/S0218127418500074

Westerberg, I. K., & McMillan, H. K. (2015). Uncertainty in hydrological signatures. *Hydrology and Earth System Sciences*, *19*(9), 3951–3968. Retrieved from https://doi.org/10.5194/hess-19-3951-2015

Westerberg, I. K., Wagener, T., Coxon, G., McMillan, H. K., Castellarin, A., Montanari, A., & Freer, J. (2016). Uncertainty in hydrological signatures for gauged and ungauged catchments. *Water Resources Research*, *52*, 1847–1865. Retrieved from https://doi.org/10.1002/2015WR017635